

# Detecting hot baryons using cross-correlation of thermal SZ maps and Weak Lensing surveys

Pranav S

The knowledge of the baryonic and non-baryonic matter distribution of the universe is fundamental in understanding evolution and structure formation in the Universe. However, a large fraction of them cannot be detected directly. One of the major ways of indirectly detecting the baryon distribution is the cross correlation between thermal Sunyaev Zel'dovich effect (tSZ) by the hot baryons and Weak Gravitational Lensing by the dark matter. There have been multiple attempts/detection of this cross-correlation in the past. However, newer and better data promises to yield better constrains as attempted in this thesis. Moreover, doing an independent analysis of this cross correlation will also be useful in detecting any systematic errors, if any, in the existing skymaps. We compute the tSZ skymaps using a methodology independent from the Planck collaboration's pipelines, and then cross correlate these skymaps with tangential shear due to lensing potential, to compare with the existing constrains on halo astrophysics and cosmology and in the process detect for the first time, hot diffuse baryons present in conglomeration of galaxies. This work consists of two parts, independent generation of tSZ skymaps using Unsupervised machine learning (which was done partially in collaboration with Prof Rishi Khatri) and cross-correlating the tSZ skymaps with RCSLenS and KiDS weak lensing surveys. Finally, we attempt to connect the observed detection with physics modelling of diffuse baryons in halos.

## I. INTRODUCTION

Though the general physical processes driving cosmological evolution and large scale structure formation is reasonably well understood, many of the details which are essential for understanding how galaxies and clusters of galaxies form and evolve are still unclear. One such important detail is the knowledge of the distribution of baryonic and dark matter in galaxies and clusters. We know that stellar mass accounts for only approximately 10% of the baryonic mass in the universe and the rest resides in diffuse components such as halos [2, 3]. This makes it hard to estimate the mass distribution of matter in galaxies and clusters. Historically, diffuse components are measured via X-Ray emissions and thermal Sunyaev-Zel'dovich effect (tSZ); but because of the sensitivity of the experiments, just relying on these will help us detect only the hot and dense diffuse components. A possible way of observing these diffuse components would be to use gravitational lensing fields; since these lensing fields provide an estimate of the matter distribution in the large scale structure of the universe. Especially, with the recent RCSLenS dataset and the ongoing KiDS dataset (??) from the galaxy surveys, weak lensing has become a precision tool in understanding large-scale structure. Whereas, our lack of understanding of baryonic physics at small scales, leads to uncertainty in our estimates of matter distribution using gravitational lensing. The missing insights from both the tSZ probes and weak lensing datasets from sky surveys can be compensated by cross-correlating tSZ probes with the weak lensing fields. Since cross-correlations also have the advantage of being immune to systematic effects which doesn't correlate with the signals, it provides a powerful method for extracting information from these probes and help us understand the astrophysical processes governing these scales.

A recent attempt at cross-correlation between the two probes found that the data supports WMAP-7yr cosmology more than the Planck Cosmology [1]. While this result was found using the tSZ maps provided by the Planck collaboration; the results beg the question of systematic deviations existing in the skymaps provided by the Planck collaboration. It is therefore useful to consider independent algorithms which extract information from the multi frequency CMB observations such as WMAP and Planck. The methodology presented by us here is the first attempt in using unsupervised machine learning to perform component separation using a model independent methodology. This work consists of 2 parts- (a) We use an independent methodology to extract the tSZ maps from Planck's frequency data. This provides us with hints, incase there exists systematic deviations from the planck skymaps. (b) We compute cross-correlations between tSZ maps and Weak Lensing maps by various sky surveys.

## II. NEW THERMAL SZ MAPS

One of the ways of removing foregrounds from our data is to have a parametric model for the foregrounds based on known physics and fit the data to these foreground models to get an estimate of the parameters and use them to eliminate the foregrounds in the data. This is the methodology followed by Commander pipeline of the Planck collaboration [9] and LIL Method [10]. These methods suffer from being model dependent and the parameters are insufficient to model the foregrounds because various physical processes contribute to the foreground in a single pixel, making it hard to model these with a single parametric model. Therefore, it is useful to look at algorithms which are model independent and just use the data to estimate the foreground characteristics.

Various such *blind* component separation algorithms have been proposed where only the spectrum of the signal is needed [11, 12] and have been applied in various variations such as Harmonic space, Needlet frame etc [13, 14]. Since these blind algorithms require the number of foreground components to be lesser than the number of spectral channels available, it is necessary to divide the sky with similar foreground properties into different regions and apply the algorithm separately on those regions to reduce the number of foreground components. These existing variations try to divide the data into different clusters with similar foregrounds based on heuristic arguments and our current understanding of the properties of the foregrounds. We provide a spectral data based approach extending upon this data driven foreground clustering approach [15], which uses the signature of the foregrounds available in the data. Since the data is clustered only based on the spectra, different regions of the sky can still be in the same cluster based on their foreground properties. To the best of our knowledge, this is the first attempt at using *unsupervised* machine learning for foreground component separation.

### A. New tSZ maps with Unsupervised Machine Learning

There have been attempts to classify the foregrounds in the data using supervised learning by using simulations to generate the training set [16]. This method involves using the simulations to generate the training data for different classes based on the different foreground models used in the simulation. We then expect the machine learning algorithm to *learn* from these simulations and help us classify the real sky into regions based on its foreground properties. This method suffers from being model dependent, similar to the parametric models of component separation as the algorithm tends to learn only based on the foreground models fed during the simulation. In order to avoid this, we use unsupervised machine learning which gives us the advantage of clustering the data in a model independent manner. In unsupervised machine learning, we take the hard clustering approach, where each data belongs only to a single class. In order to smooth the boundaries of the partitions like the current ILC algorithms, we repeat the hard clustering multiple times with different seeds. Since various seeds produce different partitions, and there is no a-priori reason to consider one partition over the other, we consider all of them with equal probability. We see that this approach essentially smoothens the boundary and no additional smoothing across the cluster boundaries are necessary.

The unsupervised machine learning algorithms used are,

- k-means clustering
- Self Organising Maps
- Auto Encoders

### B. Results

After the maps are generated using the above algorithms, We compute the power spectrum using `PolSpice` [22, 23]. The result of using the various algorithms FFP6 simulations is shown in Fig. 2. We see that our clustering algorithm is better than the one dimensional version[15]. We hope to compare it with the existing algorithms using FFP6 simulations. We also see that the neural network method like self organising map with a  $200 \times 200$  grid performs, very close to the k-means algorithm where the measures

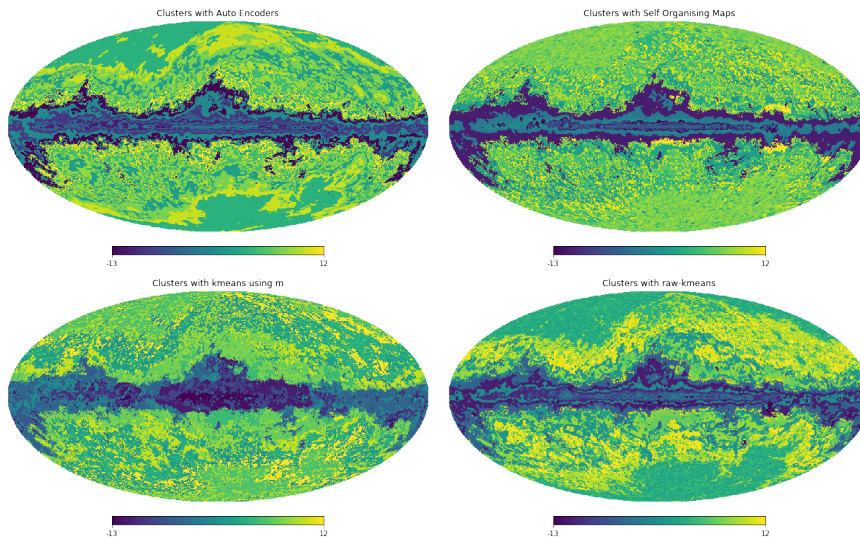


FIG. 1: A single instance Clustering of the Sky based on foregrounds using various methods (negative values indicate masked regions) In this figure, k-means refers to power spectrum of maps generated using k-means on  $m$ -values. K-means- $y$  refers do directly clustering using the foreground maps. SOM-200 refers to a self organising map with a grid size of  $200 \times 200$ .

are chosen by hand. It is interesting to note that *raw-kmeans* performs the same as a self organising map. Seeing that the k-means algorithm using the  $m$ -values as input, performs the best out of the various al-

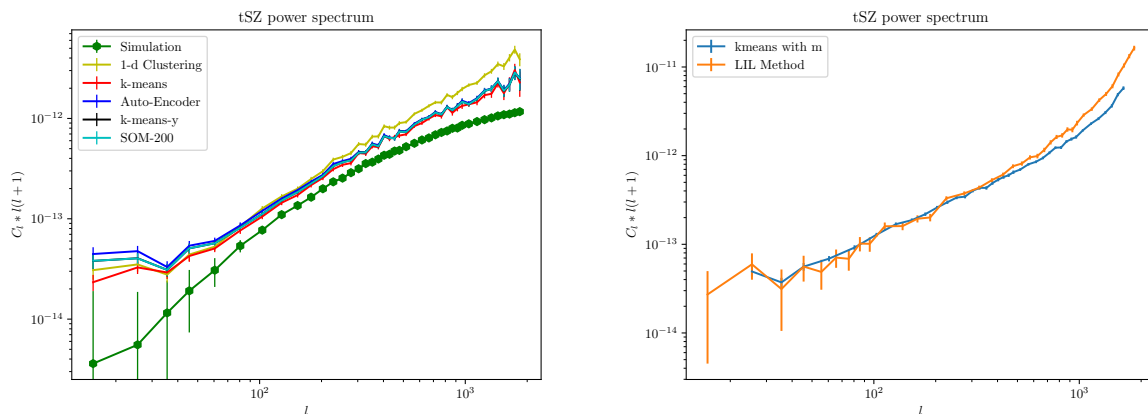


FIG. 2: (a) Comparison of the tSZ power spectrum for various methods. We see that all the other machine learning algorithms perform similarly, and better than the one parameter clustering [15]. We can also see that k-means clustering using  $m$ -values seem to perform better than the methods which involve directly using the foreground frequency maps as input (b) Comparison of the tSZ power spectrum on Planck data using Linearized Iterative Least-squares (LIL) method and k-means clustering using  $m$ -values as inputs. Considering that the large  $\ell$  exponential increase in power spectra is because of the noise, we see that the machine learning based approach performs better

gorithms explored, We use that on the frequency maps made available by the planck collaboration. From Fig. 2, We can see that the new machine learning based method performs better than the existing model based method [10]. Further analysis is necessary to understand the differences between the two maps.

### III. THERMAL-SZ WEAK LENSING CROSS CORRELATION

Cross-correlation is one of the most powerful probes available to extract the mass distribution of diffuse components in the universe. Since, cross-correlation has the advantage of being immune to systematic

effects. We attempt to utilize our new tSZ maps to extract information from the diffuse components. We compute the cross-correlation while working in the configuration space. This is because, since the galaxy skysurveys cover a small portion of the sky, the error associated with using a pseudo- $C_\ell$  method by deconvolving the mask is very high. One of the advantages of working in the configuration space is that the mask is directly taken care of, since we compute the correlation functions only in the small patches of the sky available to us. The disadvantage is the computational cost for computing the correlation functions in massive data sets.

## A. Calculation from Data

### 1. RCSLenS Survey

RCSLenS is the largest public multi-band survey, which is suitable for weak gravitational lensing measurements [24]. Its parent survey, RCS2 [25] is sub-arcsecond multiband imaging survey in the  $g, r, i, z$  bands. It covers a total area of  $785 \text{ deg}^2$ , to a depth of 24.3 mag in the r-band (for a point source at  $7\sigma$ ), carried out with a MegaCAM camera mounted on the Canada France Hawaii Telescope (CFHT). This area is divided into 14 square patches, from hereon referred to as *RCSLenS Fields*. The largest of the fields being  $100 \text{ deg}^2$  and the smallest being  $36 \text{ deg}^2$ . Each square represents a mosaic, which consists of multiple pointings of the  $1 \text{ deg}^2$  camera field of view. RCSLenS reanalyzes the data with a dedicated weak-lensing pipeline.

The RCSLenS team used the methodologies developed by the CHFTLenS team, which performed data reduction with THELI [26], Bayesian Model fitting for shear measurement using Lensfit [27], gaussianised photometry for accurate photometric redshifts [28, 29], Robust field selection based on systematic error analyses [30]. More details can be found in the original paper [24].

In order to filter out only galaxies from our data. We use the following rules,

- We remove entries with `MASK > 1`
- We only select entries with `weight > 0` and `fitclass = 0`
- We perform a magnitude cut of `magr > 18` which includes all the points in the survey.

### 2. KiDS Survey

We use the shear measurements from the Kilo Degree Survey's KiDS-450 dataset. [31–33] KiDS is an ongoing ESO optical survey which will eventually cover  $1350 \text{ deg}^2$  of the sky. Currently, the dataset covers  $449.7 \text{ deg}^2$  of the sky, in 5 different patches. It is carried out using the OmegaCAM CCD mosaic camera mounted at the Cassegrain focus of the VLT Survey Telescope. The data processing consists of ASTRO-Wise [34, 35] for data reduction from individual exposures in multiple colours to photometry, and THELI [26, 36, 37] for lensing specific data reduction of r-band images. The shears calculated using Bayesian model fitting using *lensfit* [27], and the photometric redshifts are obtained from PSF-matched photometry and calibrated using external overlapping spectroscopic surveys [28, 32]

### 3. tSZ Skymaps

For the tSZ skymaps, We use the maps generated by us as explained in the previous chapter and also the skymaps provided in the Planck 2015 Public Data Release [38]. Since tSZ skymaps are all skymaps, We use the entire skymap to compute the correlation function in order to provide a large correlation area around the RCSLenS fields, which reduces the statistical noise.

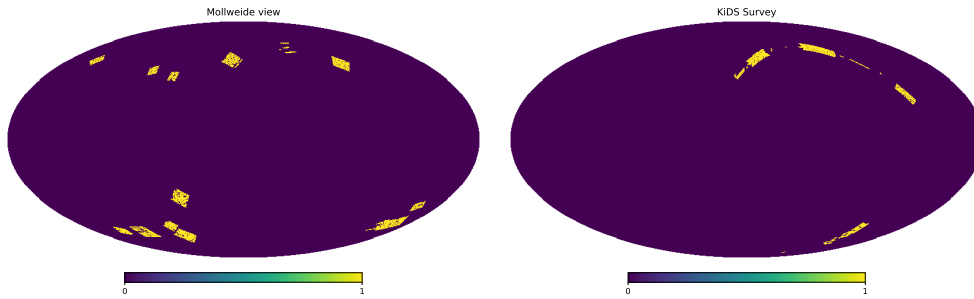


FIG. 3: A visual representation of the RCSLenS and KiDS fields, in galactic coordinates, using Mollweide projection.

### B. Two Point Correlation Functions

Now, In order to compute the two-point correlation functions we work in the configuration space. For  $y - \gamma_T$ , we compute the two point correlation function as,

$$\xi^{y-\gamma_T}(\theta) = \frac{\sum_{ij} y^i e_t^{ij} w^j \Delta_{ij}(\theta)}{\sum_{ij} w^j \Delta_{ij}(\theta)} \quad (1)$$

where,  $y^i$  is the  $y$ -value from the tSZ maps in pixel  $i$ . And  $e^{ij}$  is the tangential ellipticity of the galaxy  $j$  in the catalogue with respect to pixel  $i$ . The tangential ellipticity is corrected for both multiplicative and additive bias.  $\Delta_{ij}(\theta)$  imposes our binning scheme. It is one if the angular separation between  $i$  and  $j$  is  $\theta$  and zero otherwise, and  $w^j$  is the *lensfit* weight (For definition see Reference [39]). We compute the correlation function separately for each of the 14 RCSLenS fields or 5 KiDS fields. We then create jackknife samples of these results and then compute the mean and the standard deviation of these samples.

### C. Bias Correction

During the measurement of the ellipticities there exists calibration corrections to account for biases in our measurement. These are modelled by a multiplicative term and an additive term such that,

$$g_i^{obs} = (1 + m)g_i^{true} + c \quad (2)$$

Estimates of these biases from image simulations are given to us as part of the catalogue and we need to correct for them before computing the correlation functions. The RCSLenS catalogue contains two additive biases, Detector Bias and Noise Bias, whereas the KiDS catalogue contains only a multiplicative bias which needs to be corrected for. More information can be found in the respective catalogue information.

### D. Systematic Tests

In order to test for systematics in the data, We perform 2 systematic tests.

- **We calculate  $\langle y\gamma_x \rangle$ :** We can compute this by rotating the sources by  $45^\circ$  (ie,  $e_{1,new} = e_{2,old}$  and  $e_{2,new} = -e_{1,old}$ ). This has to be zero since  $\langle \gamma \times y \rangle = 0$  for spherically symmetric distributions.
- **We randomise the catalogue and find the correlation once again:** Since the catalogues are randomized (un-correlated), The correlation functions will become zero. Any deviations from zero, will show the existence of biases in our methodology.

in the absence of systematic errors, in our calculation. Both of these tests should give us values close to zero.

### E. Effect of Masks

Since, we are computing cross-correlations, the effect of point sources and foregrounds which are uncorrelated with the signal should not have an effect on our computations. We verify this by computing the cross-correlation with various sky masks provided by the Planck Collaboration [38]. These masks are used to avoid point sources and various other foreground contaminations in our data. We find that these masks does not have an effect on the cross-correlation computed by us.

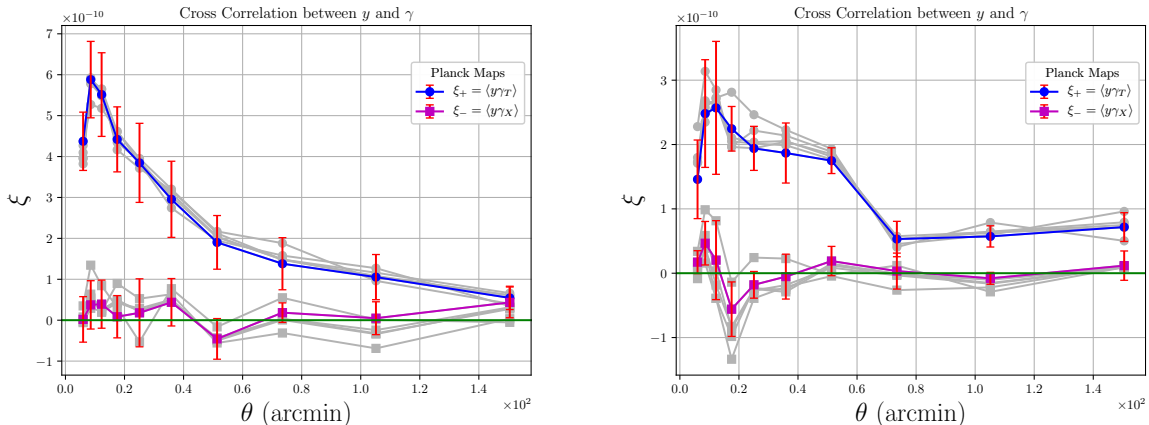


FIG. 4: We see that the masks does not play a role in the computation of cross-correlations since the foregrounds and point sources are uncorrelated with the diffuse component signal we are looking for.

### F. Results

Now, computing the cross-correlation using the Planck sky maps and our own sky maps; we get the results presented in Fig. 5. Since, as shown in Fig. 5, we see that the deviation between the two skymaps,

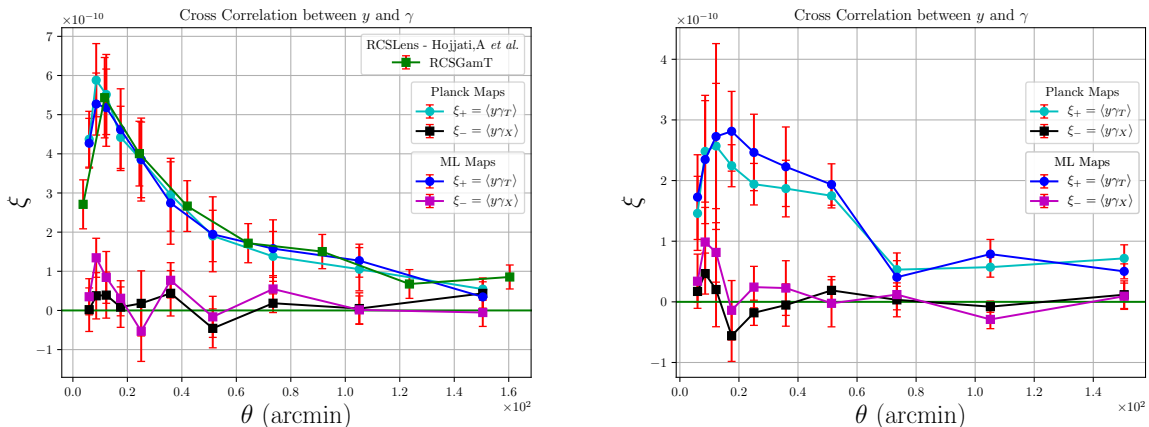


FIG. 5: (a) Cross Correlation between tSZ and Weak Lensing maps for RCSLenS fields. The two sets of data (Connected Lines) represent the *Planck skymaps* and the skymaps we generated using unsupervised machine learning techniques (ML Maps). Comparing it to the existing results, [1] our peak value seems to be smaller. (b) Cross Correlation between tSZ and Weak Lensing maps for KiDS fields. We would like to point out that since the correlations seem to agree with different skymaps, The difference could be only in systematics and uncorrelated with the signal. We would like to point out that the peak seems to be smaller and broader than the RCSLenS fields. This could be because of the fact that, the Galaxies part of the KiDS survey are closer than the RCSLenS survey

don't manifest when computing the cross-correlation functions. This is indicative of the fact that the results

can be a systematic deviation or noise uncorrelated with the signal. We would also like to point out the difference between the KiDS cross-correlation (Fig. 5) and RCSLenS cross-correlation such as a smaller peak value of the correlation and a sharper fall, which could be a artifact of the fact that the KiDS' galaxies are farther away than the RCSLenS galaxies.

### G. Comparison with theory

We like to compare our observations with theoretical predictions based on Halo models, closely following the method developed by [2]. Currently we are concentrating on computing the real space cross correlation  $\xi = \langle \gamma_T - y \rangle$ , By using

$$\xi^{y-\gamma_T}(\theta) = \int \frac{d^2\vec{l}}{2\pi^2} C_l^{y-k} \cos(2(\phi - \psi)) \exp(i\theta \cos(\phi - \psi)) \quad (3)$$

Where,  $\phi$  is the Polar angle with respect to the coordinate system and  $\psi$  is the angle between  $\vec{l}$  and the coordinate.

In order to compute the  $y - k$  cross correlation power spectra found in Eq. (3), we use the 1-halo term as defined in [40].

$$C_l^{y-k,1h} = \int_0^{z_{\max}} dz \frac{dV}{dz d\Omega} \int_{M_{\min}}^{M_{\max}} dM \frac{dn}{dM} y_l(M, z) k_l(M, z) \quad (4)$$

For the halo mass function, We use the form suggested by Sheth and Tormen [41] For the convergence profile in fourier space, We use

$$k_l = \frac{W^k(z)}{\xi^2(z)} \frac{1}{\rho_m} 4\pi \int_0^{r_{vir}} dr r^2 \frac{\sin(lr/\xi)}{lr/\xi} \rho(r; M, z) \quad (5)$$

And for the fourier transform of the projected gas pressure.

$$y_l = \frac{4\pi r_s}{l_s^2} \frac{\sigma_T}{m_e c^2} \int dx x^2 \frac{\sin(lx/\xi)}{lx/\xi} P_e(x; M, z) \quad (6)$$

For electron pressure, We use the *universal pressure profile* and the NFW model. We plan to use the best fit parameters for the Pressure profile from the Planck Collaboration and then compare the halo model predictions from both the Planck and WMAP-7yr cosmologies. To look for any non-gravitational feedback, we plan to use the method developed by [42], applied to tSZ  $C_l$ s.

## IV. CONCLUSIONS

To summarize, we now see that the various machine learning algorithms used for component separation improves upon the existing foreground clustering algorithm, whose performance was on par with the Planck Collaboration's pipelines [15]. We also see that, using unsupervised machine learning, we perform better than the model based methods too [10]. We hope to improve upon the dimensionality reduction algorithms, to eliminate the need for making a choice of variables for performing the clustering. This would in extracting the tSZ skymaps from the frequency maps in a truly model independent basis. We would also like to point out that the GILC method is robust for extracting any signal with a known spectra, and therefore our method is useful in extracting any signal in a model independent basis. We hope that using an independent algorithm to produce maps with different residuals, would be useful in testing for the effect of foregrounds and any biases in the existing algorithms for the estimates of the cosmological parameters.

We also show that, the different map generated do not have an effect on the cross correlation showing

that it is a systematic deviation which is uncorrelated with the signal. We also performed the first ever computation of cross-correlation between tSZ sky maps and weak lensing shear from the KiDS survey, which detects hot baryons. We are currently attempting to make sense of this by theoretically modelling the diffuse baryons in halos. We hope to get better constraints on halo astrophysics and cosmology, and also better understand the systematic deviations from the existing Planck sky maps.

- 
- [1] A. Hojjati et al., *Cross-correlating Planck tSZ with RCSLenS weak lensing: Implications for cosmology and AGN feedback*, *Mon. Not. Roy. Astron. Soc.* **471** (2017) 1565 [1608.07581].
- [2] Y.-Z. Ma, L. Van Waerbeke, G. Hinshaw, A. Hojjati, D. Scott and J. Zuntz, *Probing the diffuse baryon distribution with the lensing-tSZ cross-correlation*, *JCAP* **1509** (2015) 046 [1404.4808].
- [3] M. Fukugita and P. J. E. Peebles, *The Cosmic energy inventory*, *Astrophys. J.* **616** (2004) 643 [astro-ph/0406095].
- [4] S. Dodelson, *Gravitational Lensing*. Cambridge University Press, 2017, 10.1017/9781316424254.
- [5] PLANCK collaboration, P. A. R. Ade et al., *Planck 2013 results. IX. HFI spectral response*, *Astron. Astrophys.* **571** (2014) A9 [1303.5070].
- [6] K. Hornik, *Approximation capabilities of multilayer feedforward networks*, *Neural Networks* **4** (1991) 251 .
- [7] S. M. Omohundrol and S. M. Omohundro, *Five balltree construction algorithms*, 1989.
- [8] M. Jarvis, G. Bernstein and B. Jain, *The skewness of the aperture mass statistic*, *Mon. Not. Roy. Astron. Soc.* **352** (2004) 338 [astro-ph/0307393].
- [9] H. K. Eriksen et al., *CMB component separation by parameter estimation*, *Astrophys. J.* **641** (2006) 665 [astro-ph/0508268].
- [10] R. Khatri, *Linearized iterative least-squares (LIL): a parameter-fitting algorithm for component separation in multifrequency cosmic microwave background experiments such as Planck*, *Mon. Not. Roy. Astron. Soc.* **451** (2015) 3321 [1410.7396].
- [11] H. K. Eriksen, A. J. Banday, K. M. Gorski and P. B. Lilje, *Foreground removal by an internal linear combination method: Limitations and implications*, *Astrophys. J.* **612** (2004) 633 [astro-ph/0403098].
- [12] M. Remazeilles, J. Delabrouille and J.-F. Cardoso, *Foreground component separation with generalised ILC*, *Mon. Not. Roy. Astron. Soc.* **418** (2011) 467 [1103.1166].
- [13] J.-F. Cardoso, M. Martin, J. Delabrouille, M. Betoule and G. Patanchon, *Component separation with flexible models. Application to the separation of astrophysical emissions*, 0803.1814.
- [14] D. Marinucci, D. Pietrobon, A. Balbi, P. Baldi, P. Cabella, G. Kerkyacharian et al., *Spherical Needlets for CMB Data Analysis*, *Mon. Not. Roy. Astron. Soc.* **383** (2008) 539 [0707.0844].
- [15] R. Khatri, *Data driven foreground clustering approach to component separation in multifrequency CMB experiments: A new Planck CMB map*, *JCAP* **1902** (2019) 039 [1808.05224].
- [16] H. U. Norgaard-Nielsen and H. E. Jorgensen, *Foreground removal from CMB temperature maps using an MLP neural network*, *Astrophys. Space Sci.* **318** (2008) 195 [0809.2914].
- [17] F. Pedregosa et al., *Scikit-learn: Machine Learning in Python*, *J. Machine Learning Res.* **12** (2011) 2825 [1201.0490].
- [18] R. Khatri, *An alternative validation strategy for the Planck cluster catalogue and y-distortion maps*, *Astron. Astrophys.* **592** (2016) A48 [1505.00778].
- [19] M. Abadi et al., *TensorFlow: Large-Scale Machine Learning on Heterogeneous Distributed Systems*, 1603.04467.
- [20] A. Paszke, S. Gross et al., *Automatic differentiation in PyTorch*, in *NIPS Autodiff Workshop*, 2017.
- [21] P. Wittek, S. Gao, I. Lim and L. Zhao, *somoclu: An efficient parallel library for self-organizing maps*, *Journal of Statistical Software, Articles* **78** (2017) 1.
- [22] G. Chon, A. Challinor, S. Prunet, E. Hivon and I. Szapudi, *Fast estimation of polarization power spectra using correlation functions*, *Mon. Not. Roy. Astron. Soc.* **350** (2004) 914 [astro-ph/0303414].
- [23] I. Szapudi, S. Prunet and S. Colombi, *Fast clustering analysis of inhomogeneous megapixel cmb maps*, astro-ph/0107383.
- [24] H. Hildebrandt et al., *RCSLenS: The Red Cluster Sequence Lensing Survey*, *Mon. Not. Roy. Astron. Soc.* **463** (2016) 635 [1603.07722].
- [25] D. G. Gilbank, M. D. Gladders, H. K. C. Yee and B. C. Hsieh, *The Red-sequence Cluster Survey-2 (RCS-2): Survey Details and Photometric Catalog Construction*, *Aj* **141** (2011) 94 [1012.3470].
- [26] T. Erben, H. Hildebrandt, L. Miller, L. van Waerbeke, C. Heymans, H. Hoekstra et al., *CFHTLenS: the Canada–France–Hawaii Telescope Lensing Survey – imaging data and catalogue products*, *Monthly Notices of the Royal Astronomical Society* **433** (2013) 2545 [http://oup.prod.sis.lan/mnras/article-pdf/433/3/2545/13761746/stt928.pdf].
- [27] L. Miller, C. Heymans, T. D. Kitching, L. van Waerbeke, T. Erben, H. Hildebrandt et al., *Bayesian galaxy shape measurement for weak lensing surveys – III. Application to the Canada–France–Hawaii Telescope Lensing Survey*, *Monthly Notices of the Royal Astronomical Society* **429** (2013) 2858

- [<http://oup.prod.sis.lan/mnras/article-pdf/429/4/2858/3268972/sts454.pdf>].
- [28] H. Hildebrandt, T. Erben, K. Kuijken, L. van Waerbeke, C. Heymans, J. Coupon et al., *CFHTLenS: improving the quality of photometric redshifts with precision photometry\**, *Monthly Notices of the Royal Astronomical Society* **421** (2012) 2355 [<http://oup.prod.sis.lan/mnras/article-pdf/421/3/2355/5838743/mnras0421-2355.pdf>].
- [29] N. Benitez, *Bayesian photometric redshift estimation*, *The Astrophysical Journal* **536** (2000) 571.
- [30] C. Heymans, L. van Waerbeke, L. Miller, T. Erben, H. Hildebrandt, H. Hoekstra et al., *CFHTLenS: the Canada–France–Hawaii Telescope Lensing Survey*, *Monthly Notices of the Royal Astronomical Society* **427** (2012) 146 [<http://oup.prod.sis.lan/mnras/article-pdf/427/1/146/18231420/427-1-146.pdf>].
- [31] K. Kuijken et al., *Gravitational Lensing Analysis of the Kilo Degree Survey*, *Mon. Not. Roy. Astron. Soc.* **454** (2015) 3500 [1507.00738].
- [32] H. Hildebrandt et al., *KiDS-450: Cosmological parameter constraints from tomographic weak gravitational lensing*, *Mon. Not. Roy. Astron. Soc.* **465** (2017) 1454 [1606.05338].
- [33] I. Fenech Conti, R. Herbonnet, H. Hoekstra, J. Merten, L. Miller and M. Viola, *Calibration of weak-lensing shear in the Kilo-Degree Survey*, *Mon. Not. Roy. Astron. Soc.* **467** (2017) 1627 [1606.05337].
- [34] E. A. Valentijn et al., *Astro-WISE: Chaining to the Universe*, *ASP Conf. Ser.* **376** (2006) 491 [astro-ph/0702189].
- [35] K. Begeman, A. N. Belikov, D. R. Boxhoorn and E. A. Valentijn, *The astro-wise datacentric information system*, *Experimental Astronomy* **35** (2013) 1.
- [36] M. Schirmer, *THELI: CONVENIENT REDUCTION OF OPTICAL, NEAR-INFRARED, AND MID-INFRARED IMAGING DATA*, *The Astrophysical Journal Supplement Series* **209** (2013) 21.
- [37] T. Erben, M. Schirmer, J. P. Dietrich, O. Cordes, L. Habertzettl, M. Hettterscheidt et al., *Gabods: The garching-bonn deep survey*, *Astronomische Nachrichten* **326** (2005) 432 [<https://onlinelibrary.wiley.com/doi/pdf/10.1002/asna.200510396>].
- [38] PLANCK collaboration, N. Aghanim et al., *Planck 2015 results. XXII. A map of the thermal Sunyaev-Zeldovich effect*, *Astron. Astrophys.* **594** (2016) A22 [1502.01596].
- [39] L. Miller, C. Heymans, T. D. Kitching, L. van Waerbeke, T. Erben, H. Hildebrandt et al., *Bayesian galaxy shape measurement for weak lensing surveys – III. Application to the Canada–France–Hawaii Telescope Lensing Survey*, *Monthly Notices of the Royal Astronomical Society* **429** (2013) 2858 [<http://oup.prod.sis.lan/mnras/article-pdf/429/4/2858/3268972/sts454.pdf>].
- [40] A. Cooray and R. K. Sheth, *Halo Models of Large Scale Structure*, *Phys. Rept.* **372** (2002) 1 [astro-ph/0206508].
- [41] R. K. Sheth and G. Tormen, *An Excursion Set Model of Hierarchical Clustering: Ellipsoidal Collapse and the Moving Barrier*, *Mon. Not. Roy. Astron. Soc.* **329** (2002) 61 [astro-ph/0105113].
- [42] A. Iqbal, S. Majumdar, B. B. Nath, S. Ettori, D. Eckert and M. A. Malik, *Excess entropy and energy feedback from within cluster cores up to  $r_{200}$* , *Mon. Not. Roy. Astron. Soc.* **472** (2017) 713 [1703.00028].